This is a repository copy of *Accurate Reconstruction and Suppression for Azimuth Ambiguities in Spaceborne Stripmap SAR Images*.

eprints@whiterose.ac.uk
https://eprints.whiterose.ac.uk/

# Accurate Reconstruction and Suppression for Azimuth Ambiguities in Spaceborne Stripmap SAR Image

Jie Chen, Member, IEEE, Kai Wang, Student Member, IEEE, Wei Yang, Member, IEEE, and

Wei Liu, Senior Member, IEEE

**Abstract—In this paper, an accurate mathematical model for azimuth ambiguity in stripmap Synthetic Aperture Radar (SAR) image is first constructed, with an azimuth ambiguity factor (AAF) defined as the residual amplitude and phase terms of ambiguities. Next, a novel framework for reconstructing and suppressing azimuth ambiguity is proposed based on analysis of the AAF. In this framework, azimuth ambiguities are accurately reconstructed by applying reconstruction filters in the range Doppler and 2-D frequency domain, and then, the reconstructed signal is used for suppressing azimuth ambiguities. Moreover, the proposed framework does not depend on the statistical characteristics of the SAR image and is capable of reducing the space-variant ambiguities. As verified by both simulated data and real TerraSAR-X data, the proposed method is capable of suppressing azimuth ambiguities in SAR images.**

**Index Terms—Ambiguity Reconstruction, Ambiguity Suppression, Azimuth Ambiguities, Synthetic Aperture Radar.**

## I. INTRODUCTION

THE quality of spaceborne Synthetic Aperture Radar (SAR) images is likely to be significantly degraded because of azimuth ambiguities [1]. To suppress azimuth ambiguity, some methods have been proposed, e.g., ideal filters, Wiener filters, and the inpainting technique [2]–[5].

The ideal filter approach is an excellent strategy that involves generating a two-dimensional reference function for the SAR processing that provides (in addition to the matched filter for the signal within the bandwidth) the deconvolution of the extra contribution from the aliased ambiguities signal [2]. However, an ideal filter fails to address space-variant ambiguities and is not suitable for those caused by distributed targets.

Based on the spectral characteristics, Wiener-filter-based methods have been proposed to suppress azimuth ambiguities [3]–[5]. These methods do not explore accurate modelling of ambiguities, and they are proposed based on the statistical characteristics of the spectra in the SAR image. These methods can suppress ambiguities but suffer from resolution degradation. Moreover, the strong dependence on spectral differences between the aliased antenna pattern and mainlobe pattern within the bandwidth is also a limiting factor for such methods.

The inpainting technique is another effective technique [6]. Through inpainting, ambiguities can be completely removed, but targets covered by ambiguities are also lost.

Currently, azimuth ambiguity suppression research mainly focuses on statistical features and lacks accurate modelling of the principle of ambiguity generation. In [1], R. K. Raney showed that the wavelength, pulse repetition frequency (PRF), processing bandwidth and incorrect range migration (RM) are all responsible for azimuth ambiguities in SAR image; however, further analysis was not provided.

Ambiguities are fundamentally caused by signal aliasing, and imaging processing also affects their behaviour. In this paper, an accurate ambiguity model is established in which the mathematical formulation for azimuth ambiguities is derived based on signal aliasing. Exploring the residual amplitude and phase terms of ambiguities, the azimuth ambiguity factor (AAF) is defined to quantitatively describe the corrupting effect of ambiguities; this term can also be regarded as a new system index concerning azimuth ambiguity.

In the AAF, there are five factors affecting ambiguities: the ambiguity antenna pattern, ambiguity range cell migration (ARCM), secondary range compression (SRC) error, azimuth defocusing factor, and the constant fractional sampling phase (see [2] for details). Based on the AAF analysis, a reconstruction and suppression framework for azimuth ambiguity is proposed. Through several compensation filters in the range Doppler and 2-D frequency domain, the ambiguities are reconstructed using the original targets; and then, azimuth ambiguities in the SAR image can be effectively cancelled with the help of the reconstructed signal. Finally, the proposed framework is tested on both simulated and real data.

The remainder of this paper is organized as follows. Detailed analysis of the ambiguity phenomenon is given in Section II,

and a suppression method is proposed in Section III. Section IV presents the experimental results, and conclusions are drawn in Section V.

## II. PRINCIPLE OF AZIMUTH AMBIGUITY

Fig. 1 illustrates the geometry for azimuth ambiguities in spaceborne SAR, where only the first pair of ambiguity is shown. The middle target is the real target responsible for ambiguities, denoted as the "original target". In the following sections, the left ambiguity target is denoted as the +1 ambiguity, whereas the right one is referred to as the -1 ambiguity.
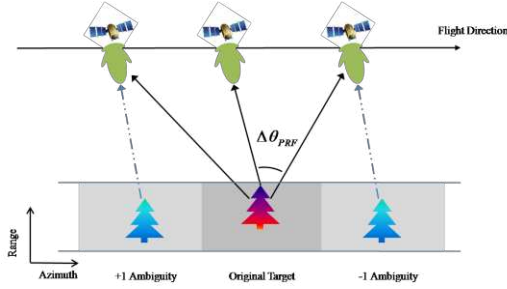


Fig. 1. Geometry for azimuth ambiguities.

### A. Ambiguity Range Cell Migration (ARCM)

Fig. 2 shows the migration curves of two targets in the range Doppler domain: $\Omega_{ref}$ and $\Omega_0$. $\Omega_{ref}$ is located at the reference range position, whereas $\Omega_0$ is not. Before imaging processing, the uncorrected RM curve of $\Omega_{ref}$ is the arc $J_{ref} A_{ref} K_{ref}$, as shown by the blue dashed line. However, the limited $f_p$, which denotes the PRF, separates the curve into two parts: arcs $C_{ref} I_{ref}$ and $E_{ref} I_{ref}$. $C_{ref} I_{ref}$ is the arc for the original target, whereas $E_{ref} I_{ref}$ is the aliased part of $J_{ref} A_{ref} K_{ref}$, representing the energy of the -1 ambiguity. After range cell migration correction (RCMC), $C_{ref} I_{ref}$ is transformed into a vertical line ($B_{ref} H_{ref}$), whereas the ambiguity curve remains a slanting segment ($D_{ref} H_{ref}$). Comparing targets $\Omega_0$ and $\Omega_{ref}$, the azimuth ambiguities are found to be space-variant.
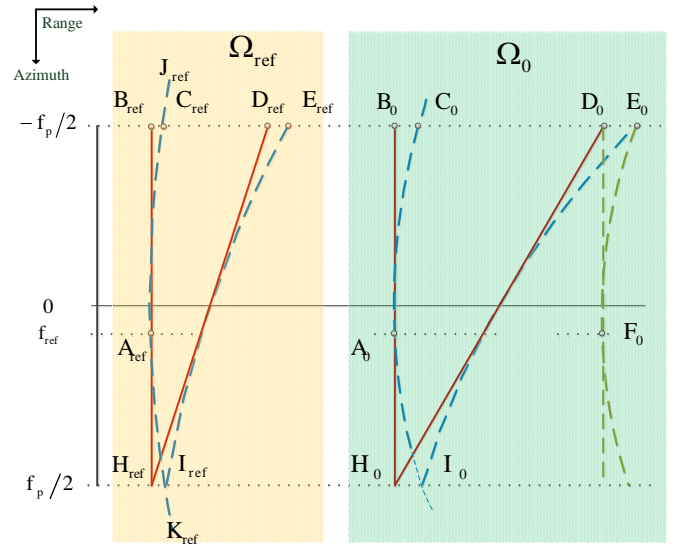


Fig. 2. RM of the original target and corresponding -1 ambiguity in the range Doppler domain. Through RCMC, the original target has been transformed into a vertical line, whereas the ambiguity is still a slanting line.

### B. Impact of Imaging Processing on Ambiguities

In stripmap mode, the echo of the original target in the 2-D frequency domain can be expressed as follows [7]:

$$S_0^{Ech}\left(f_\tau, f_\eta\right) = W_r\left(f_\tau\right) \cdot W_a\left(f_\eta - f_{ref}\right) \cdot \exp\left\{-j4\pi R_0 D\left(f_\eta\right)/\lambda\right\}$$
$$\cdot \exp\left\{-j\frac{\pi}{K_m\left(f_\eta\right)} f_\tau^2\right\} \cdot \exp\left\{-j\frac{4\pi R_0}{cD\left(f_\eta\right)} f_\tau\right\} \cdot \exp\left\{-j2\pi f_\eta t_c\right\} \quad (1)$$

where $f_\tau$ is the range frequency, $f_\eta$ is the azimuth frequency, $f_{ref}$ is the Doppler centroid frequency, $W_r\left(\square\right)$ is the range antenna pattern, $W_a\left(\square\right)$ is the azimuth antenna pattern, $R_0$ is the shortest range of the selected target, $c$ is the light velocity, $t_c$ represents the azimuth position of target, $K_m$ is the Doppler frequency modulation rate, $\lambda$ is the wavelength, and $D$ is the RM factor (see [7]).

Because of the limited azimuth sampling, the high-frequency spectrum is aliased to the baseband, leading to the presence of azimuth ambiguity. As a result, the expression of the -1 ambiguity can be written as

$$S_{-1}^{Ech}\left(f_\tau, f_\eta\right) = S_0^{Ech}\left(f_\tau, f_\eta - f_p\right) \quad (2)$$

After SAR imaging processing, the signal expression of original target and ambiguity can be written as

$$S_0^{Ima}\left(f_\tau, f_\eta\right) = W_r\left(f_\tau\right) \cdot W_a\left(f_\eta - f_{ref}\right) \cdot \exp\left\{-j\frac{4\pi R_0}{cD\left(f_{ref}\right)} f_\tau\right\}$$
$$\cdot \exp\left\{-j2\pi f_\eta t_c\right\}$$
$$S_{-1}^{Ima}\left(f_\tau, f_\eta\right) = W_r\left(f_\tau\right) \cdot W_a\left(f_\eta - f_{ref} - f_p\right) \quad (3)$$
$$\cdot \exp\left\{-j4\pi R_0 Q_1\left(f_\eta\right) f_\tau/c\right\} \cdot \exp\left\{jQ_2\left(f_\eta\right) f_\tau^2\right\}$$
$$\cdot \exp\left\{j4\pi R_0 Q_3\left(f_\eta\right)/\lambda\right\} \cdot \exp\left\{-j2\pi f_\eta t_c\right\} \cdot \exp\left\{j\theta_c\right\}$$

where

$$Q_2\left(f_\eta\right) = \frac{\pi D\left(f_\eta\right)}{K_m\left(f_\eta\right) D\left(f_{ref}\right)} - \frac{\pi D\left(f_\eta\right)}{K_m\left(f_\eta - f_p\right) D\left(f_{ref}\right)} \quad ,$$

$$Q_1\left(f_\eta\right)=\frac{D\left(f_\eta\right)}{D\left(f_\eta-f_p\right)D\left(f_{ref}\right)} \ , \ Q_3\left(f_\eta\right)=\frac{D^2\left(f_\eta\right)}{D\left(f_\eta-f_p\right)}-D\left(f_\eta-f_p\right)$$

$\theta_c=\mathrm{mod}\left(2\pi f_p t_c, 2\pi\right)$ , and $\mathrm{mod}(\square)$ denotes the modular operation. Note that by employing 2-D IFFT in (3), a focused original target can be derived, whereas the azimuth ambiguous targets turn out to be not well-focused.

In (3), $\exp\left\{-j4\pi R_0 Q_1\left(f_\eta\right)f_\tau/c\right\}$ represents the ARCM, where ambiguity energy is not in one range bin, i.e., the phase of this term is still related to the azimuth frequency $f_\eta$ . Moreover, the quadratic SRC phase exists in the range, which is denoted by $\exp\left\{jQ_2\left(f_\eta\right)f_\tau^2\right\}$ . The term $\exp\left\{j4\pi R_0 Q_3\left(f_\eta\right)/\lambda\right\}$ represents the residual azimuth phase, which is caused by the mismatched azimuth compression for ambiguity. The last term, $\exp\left\{j\theta_c\right\}$ , is a constant phase term.

### C. Azimuth Ambiguity Factor (AAF)

Taking (3) into account, compared to the focused original target, the residual amplitude and phase terms of the ambiguities can be defined as the AAF:

$$\mathrm{AAF}\left(f_\tau, f_\eta\right)=W_a\left(f_\eta-f_{ref}-f_p\right)\cdot\exp\left\{-j4\pi R_0 Q_1\left(f_\eta\right)f_\tau/c\right\}$$
$$\cdot\exp\left\{jQ_2\left(f_\eta\right)f_\tau^2\right\}\cdot\exp\left\{j4\pi R_0 Q_3\left(f_\eta\right)/\lambda\right\}\cdot\exp\left\{j\theta_c\right\} \quad (4)$$

The AAF is found to contain five factors: the ambiguity antenna pattern, ARCM, SRC error, azimuth defocusing factor, and the constant phase. In fact, the appearance of ambiguity is entirely determined by these factors.

### III. AMBIGUITY RECONSTRUCTION AND SUPPRESSION

Because the AAF is defined as the residual amplitude and phase terms of ambiguities, based on the AAF, we are able to reconstruct the ambiguity using original targets; the reconstructed signal can then be used to suppress ambiguities in the original SAR image. The reconstruction method can be divided into 4 stages:

a). Compensate the antenna pattern of ambiguity. b). Reconstruct the uncorrected RM curve. c). Compensate the SRC error. d). Reconstruct the final azimuth phase of ambiguity.

Once the four stages are completed, we can derive the reconstructed ambiguities. Fig. 3 shows the flow chart of the proposed reconstruction framework.

First, the azimuth phase history of ambiguity is compensated to the original target by

$$H_{az\_pha}=\exp\left\{-j4\pi R_0 D\left(f_\eta-f_p\right)/\lambda\right\} \quad (5)$$

Similarly, antenna pattern compensation can be applied to reconstruct the spectrum of the ambiguities:

$$H_{az\_ant}=\frac{W_a\left(f_\eta-f_{\eta c}-f_p\right)}{W_a\left(f_\eta-f_{\eta c}\right)} \quad (6)$$

where $W_a$ is the azimuth antenna pattern in the azimuth frequency domain [7].

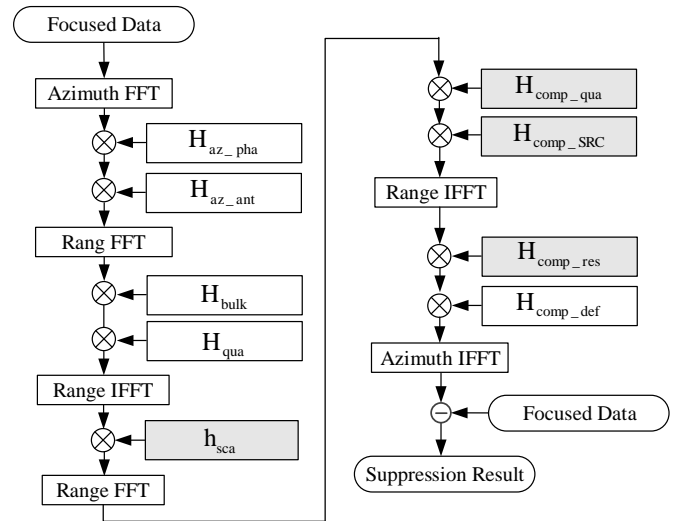The following steps concentrate on ARCM reconstruction.



Fig. 3. Flow chart of the proposed framework.

The total ARCM is

$$\mathrm{ARCM}_{total}\left(R_0, f_\eta\right)=R_0 Q_1\left(f_\eta\right)-R_0/D\left(f_{ref}\right) \quad (7)$$

Note that, ARCM is a linear function regarding range cells that is suitable for the chirp scaling operation.

Similar to the RCMC operation in chirp scaling algorithm, the ARCM can be separated into two parts: a "bulk ARCM" that represents the ARCM of the target in the reference range cell and a "differential ARCM" that represents the remainder. The bulk ARCM is constant for all targets, while the differential ARCM is range-variant.

$$\mathrm{ARCM}_{bulk}\left(R_0, f_\eta\right)=R_{ref}Q_1\left(f_\eta\right)-R_{ref}/D\left(f_{ref}\right)$$
$$\mathrm{ARCM}_{diff}\left(R_0, f_\eta\right)=\mathrm{ARCM}_{total}\left(R_0, f_\eta\right)-\mathrm{ARCM}_{bulk}\left(R_0, f_\eta\right) \quad (8)$$
$$=\left(R_0-R_{ref}\right)\left[Q_1\left(f_\eta\right)-1/D\left(f_{ref}\right)\right]$$

The bulk ARCM can be reconstructed by a linear phase function in the range frequency domain. The differential ARCM varies with range and is zero at $R_0=R_{ref}$ ; the differential ARCM can be corrected by a chirp scaling operation in the range time domain. (Details on the principle of chirp scaling operation can be found in [7].)

The implementation of ARCM reconstruction can be divided into five steps.

Step 1: Range FFT is employed, and a linear phase function is applied to reconstruct the bulk ARCM:

$$H_{bulk}=\exp\left\{-j\frac{4\pi}{c}R_{ref}\left[Q_1\left(f_\eta\right)-\frac{1}{D\left(f_{ref}\right)}\right]f_\tau\right\} \quad (9)$$

Step 2: A quadratic phase is added to the signal in the 2-D frequency domain:

$$H_{qua}=\exp\left\{-j\frac{\pi}{K_{new}}f_\tau^2\right\} \quad (10)$$

where $K_{new}$ is the Doppler frequency modulation rate.

Step 3: Returning to the range Doppler domain, in accordance with the differential ARCM in (8), the signal is multiplied by a scaling function:

$$h_{sca} = \exp\left\{ j\pi K_{new} \alpha \left( \tau - 2R_{ref} Q_1 \left( f_\eta \right) / c \right)^2 \right\} \tag{11}$$

where $\alpha = \dfrac{1}{D\left( f_{ref} \right) Q_1 \left( f_\eta \right)} - 1$.

Step 4: The quadratic phase in the signal can be cancelled in the 2-D frequency domain. Note that because of the scaling function $h_{sca}$, the Doppler frequency modulation rate has been changed from $K_{new}$ to $(1+\alpha) \cdot K_{new}$ [7]:

$$H_{comp\_qua} = \exp\left\{ j \frac{\pi}{K_{new}(1+\alpha)} f_\tau^2 \right\} \tag{12}$$

Simultaneously, the extra phase caused by the SRC error is also reconstructed by $H_{comp\_SRC}$:

$$H_{comp\_SRC} = \exp\left\{ -jQ_2 \left( f_\eta \right) f_\tau^2 \right\} \tag{13}$$

Step 5: Returning to the range Doppler domain, the residual phase introduced by the chirp scaling operation is compensated by $H_{comp\_res}$:

$$H_{comp\_res} = \exp\left\{ -j\pi K_{new} \frac{4}{c^2} \left( \frac{R_0}{Q_1 \left( f_\eta \right) D \left( f_{ref} \right)} - \frac{R_{ref}}{D \left( f_{ref} \right)} \right)^2 \frac{\alpha}{1+\alpha} \right\} \tag{14}$$

At this stage, the ARCM in all the range cells has been reconstructed. Furthermore, because the azimuth compensation function is designed for the radar echo of the original target, it results in the defocusing phase for ambiguity, which can be introduced using $H_{comp\_def}$:

$$H_{comp\_def} = \exp\left\{ j4\pi R_0 Q_1 \left( f_\eta \right) D \left( f_\eta \right) D \left( f_{ref} \right) / \lambda \right\} \tag{15}$$

After Azimuth IFFT, the ambiguities are fully reconstructed in the corresponding position. As a result, the reconstructed signal can be used to cancel the ambiguities in the original SAR image.

The computational complexity of the proposed method is nearly twice the complexity of the ideal filter. However, considering that the azimuth ambiguity suppression method is a post-processing technique (which usually does not have a strict requirement for real-time processing), we suggest that the computational complexity of the proposed framework is acceptable for many applications.

In addition, the proposed framework is designed for the first-order azimuth ambiguity. To address the high-order ambiguities using the proposed framework, a more accurate mathematical expression of ambiguities is first required, and the reconstruction algorithm should be improved to adjust the complicated ambiguity component.

## IV. EXPERIMENTAL RESULTS

### A. Implementation with Simulated Data

A simulation with 9 point targets is performed using the parameters listed in Table I. Fig. 4(a) shows the imaging result in the presence of azimuth ambiguities; these ambiguity blocks are the ambiguities of 9 original targets, respectively. Because the total image is too large to accommodate, for simplicity, only the -1 ambiguity area is shown in the figure; the original targets are not present. The magnified patch of the upper left ambiguity

indicates that the blurring area has a size of $35 \times 30$, i.e., 35 pixels in azimuth and 30 pixels in range. The azimuth size is slightly larger than the range size, while the range size is approximately equal to the ARCM value (29 pixels derived using AAF analysis).
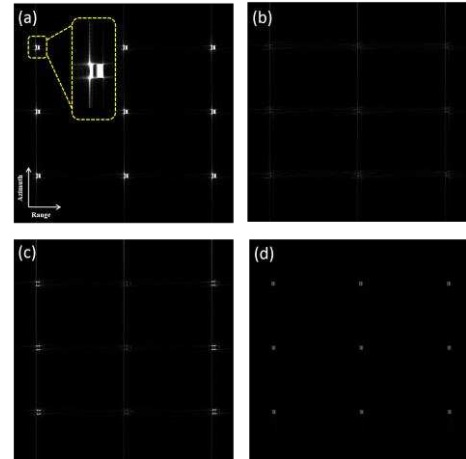
TABLE I
PARAMETERS OF TERRASAR-X DATASET S



Fig. 4. Ambiguity suppression experiment for point targets: (a) -1 ambiguities and magnified patch showing the details of the upper left ambiguity; (b) suppression result using the proposed framework; (c) suppression result using the ideal filter; (d) suppression result using Wiener filter.
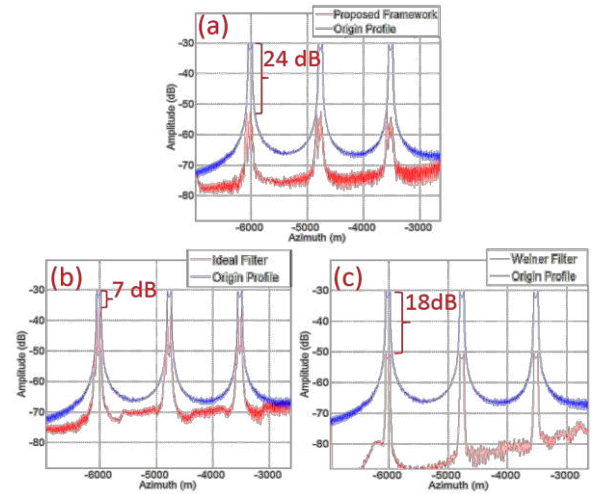


Fig. 5. Profiles of left three targets and their ambiguities: (a) the ambiguity suppression ratio is 24 dB using the proposed framework; (b) the suppression ration is 7 dB for the ideal filter method; (c) the Wiener filter achieves a suppression ratio of 18 dB.

| Parameter | Value | Parameter | Value |
|---|---|---|---|
| Wavelength | 0.0313 m | Slant Range Resolution | 1.18 m |
| Reference Range | 615172 m | Azimuth Resolution | 3.3 m |
| PRF | 3551. 13Hz | Range Pixel Spacing | 0.91 m |
| Sampling Frequency | 165 MHz | Azimuth Pixel Spacing | 2.08 m |
| Equivalent Velocity | 7383 m/s | MultiLooks | 1×1 |

Fig. 4(b) shows that the 9 ambiguities have already been removed by proposed framework, whereas some artefacts still exist using the ideal filter and Wiener filter approach as shown in Figs. 4(c) and (d).

Fig. 5 shows the profile of the left three point targets and the corresponding ambiguities. The ambiguities are found to be effectively suppressed by the proposed framework, with a 24 dB performance, i.e., better than the 7 dB result by the ideal filter and the 18 dB result by the Wiener filter.

Fig. 6 shows the covered targets recovery experiment, where the proposed method, ideal filter and Wiener filter are applied for ambiguity suppression. In this case, after imaging processing, a small dinghy is covered by the ambiguities of a large ship with strong backscattering, and the average intensity of the small dinghy is as large as the ambiguities located in the same area. Fig. 6(a2) shows the small dinghy,
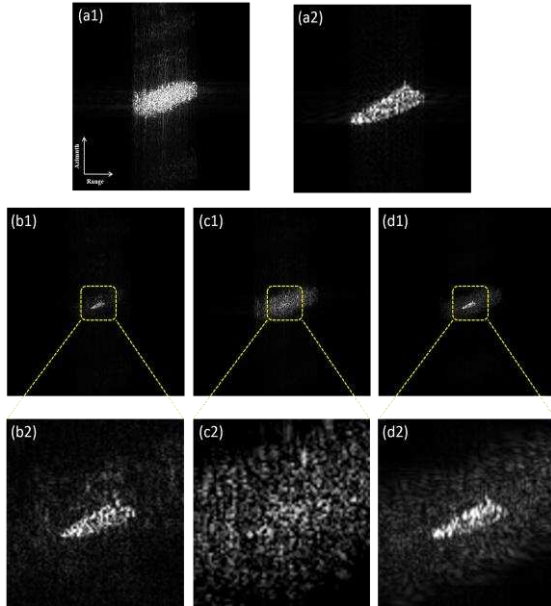


Fig. 6. Experimental results for covered targets: (a1) the small dinghy is covered by the ambiguities of a large ship; (a2) The small dinghy without ambiguities present; (b1) processed result using the proposed framework; (b2) magnified patch of the scene centre; (c1) processed result using the ideal filter; (c2) magnified patch of the scene centre; (d1) processed result using the Wiener filter method; (d2) magnified patch of the scene centre.

but it is covered by the ambiguities in Fig. 6(a1). Figs. 6(b1), (c1), and (d1) are the processed results obtained using the proposed framework, the ideal filter and the Wiener filter, respectively. Figs. 6(b2), (c2), and (d2) are the magnified patches for the corresponding methods. After the use of the proposed method and the Wiener filter, the covered dinghy can be detected against the background. The proposed framework suppresses ambiguities to a lower level and produces a better result with less loss of resolution. The suppression ratio of the proposed method is 18.0 dB, whereas that of the ideal filter is 6.8 dB and that of the Wiener filter is 13.5 dB.

### B. Implementation with Real TerraSAR-X Data

The proposed method is also used to suppress the distributed ambiguities in the image of a Dubai coastal area acquired by TerraSAR-X. This case concerns the ambiguities of a ship, where the ambiguity area is indicated by the yellow rectangular box in Fig. 7(a). Fig. 7(b) shows the reconstructed ambiguities, which are found to have already been generated at the positions where original ambiguities are located. As shown by the high

image quality result in Fig. 7(c), the ambiguity intensity has been suppressed to a relatively low level by our proposed framework. For this case, the suppression ratio of the proposed framework is 7.2 dB, whereas that of the ideal filter is 2.9 dB and that of the Wiener filter is 5.8 dB.
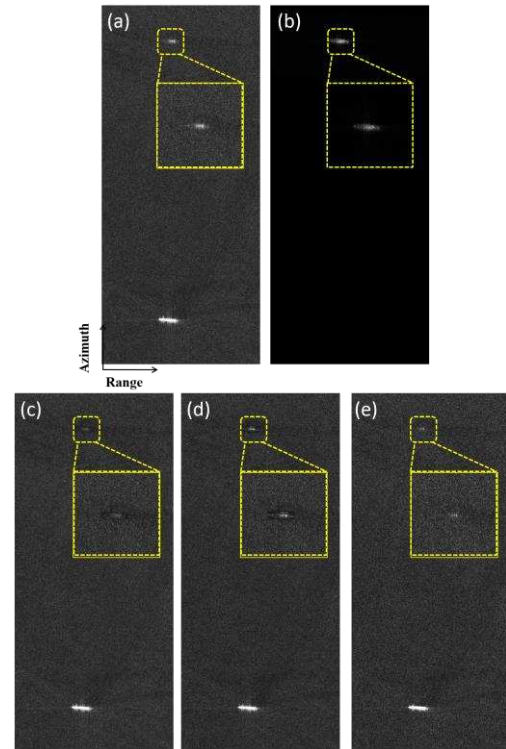


Fig. 7. Experimental results for the ambiguities caused by a ship: (a) original image; (b) reconstructed ambiguities using the proposed framework; (c) processed result using the proposed framework; (d) result using the ideal filter method.

## V. CONCLUSION

A novel framework based on accurate reconstruction modelling was proposed for the suppression of azimuth ambiguities in spaceborne stripmap SAR image. An analysis of the generation of azimuth ambiguities was first provided, and the AAF was defined based on the residual amplitude and phase terms of the ambiguities. The key concept of the proposed method is to reconstruct the ambiguities using the original target so that the ambiguities in the original image can be removed. The proposed method is based on accurate ambiguity signal analysis, does not rely on the statistical characteristics of the azimuth spectrum, and can be applied to suppress space-variant azimuth ambiguities. As demonstrated by the experimental results, the proposed method can effectively suppress the existing azimuth ambiguities in SAR image.

### REFERENCES

[1]  R. K. Raney, and G. J. Princz, "Reconsideration of azimuth ambiguities in SAR," IEEE Trans. Geosci. Remote Sens., vol. GE-25, no. 6, pp. 783–787, Nov. 1987.

[2]  A. Moreira, "Suppressing the azimuth ambiguities in synthetic aperture radar images," IEEE Trans. Geosci. Remote Sens., vol. 31, no. 4, pp. 885–895, Jul. 1993.

[3]  A. M. Guarnieri, "Adaptive removal of azimuth ambiguities in SAR images," IEEE Trans. Geosci. Remote Sens., vol. 43, no. 3, pp. 625–633, Mar. 2005.

[4]  G. D. Martino, A. Iodice, D. Riccio, and G. Ruello, "Filtering of azimuth ambiguity in stripmap synthetic aperture radar images," IEEE J. Sel. Topics Appl. Earth Observ. in Remote Sens., vol. 7, no. 9, pp. 3967–3978, Sep. 2014.

[5]  M. Villano, and G. Krieger, "Spectral-based estimation of the local azimuth ambiguity-to-signal ratio in SAR images," IEEE Trans. Geosci. Remote Sens., vol. 52, no. 5, pp. 2304–2313, May 2014.

[6]  J. Chen, M. Iqbal, W. Yang, P. B. Wang, and B. Sun, "Mitigation of azimuth ambiguities in spaceborne stripmap SAR images using selective restoration," IEEE Trans. Geosci. Remote Sens., vol. 52, no. 7, pp. 4038–4045, Jul. 2014.

[7]  I. G. Cumming, and F. H. Wong, Digital Processing of Synthetic Aperture Radar Data: Algorithms and Implementation. London: Artech House, 2004.